Int. J. Electrochem. Sci., 14 **(2019)** 8852 – 8868, doi: 10.20964/2019.09.24

International Journal of
ELECTROCHEMICAL
SCIENCE
www.electrochemsci.org

Synthesis, Characterization and Corrosion Inhibition Performance of the Thiourea-chitosan in Acidic Medium

Meng Wang[1], *Jing Zhang*[1,2,*], *Qinghai Wang*[1], *Min Du*[1,2]

[1] College of Chemistry and Chemical Engineering, Ocean University of China, 266100, Qingdao, China
[2] Key Laboratory of Marine Chemistry Theory and Technology, Ministry of Education， 266100, Qingdao, China
[*]E-mail: dmh217@ouc.edu.cn

Received: 23 March 2019/ *Accepted:* 4 May 2019 / *Published:* 31 July 2019

The water-soluble and green thiourea-chitosan (TUCTS) was synthesized and characterized by the Fourier transform infrared spectroscopy (FT-IR) and elemental analysis method. The corrosion inhibition performance and behavior of TUCTS for Q235 steel in 1 mol·L^{-1} HCl were investigated by weight loss method, surface morphology analysis, potentiodynamic polarization curves and electrochemical impedance spectroscopy (EIS). It is found that the synthesized TUCTS is an excellent corrosion inhibitor and the inhibition efficiency exceeds 90% at 25℃. The inhibitor acts as a mixed type inhibitor by geometrical blanketing effect. Thermodynamics analysis demonstrates that the adsorption of TUCTS on Q235 steel surface fit in with the Langmuir model. The adsorption type is both physical and chemical adsorption but chemisorption dominates.

Keywords: Thiourea-chitosan, corrosion inhibitor, acid corrosion

1. INTRODUCTION

Hydrochloric acid is extensively used in the pickling industry to remove rust and scale from metal surface. However, hydrochloric acid is one of the most common corrosive medium which results in the tremendous damage of metallic matrix [1, 2]. The problem of hydrochloric acid corrosion has led to the development of corrosion protection methods. Among these methods, adding corrosion inhibitor has been proven to be the simplest and most practical method [3, 4, 5]. The huge usage of inhibitor is attributed to its advantages, which including lower investment and quick effect. Many studies about organic corrosion inhibitors used for mitigating hydrochloric acid corrosion have already been reported. But most organic inhibitors would jeopardize environment [6, 7]. Hence, the study on corrosion inhibitor is developing towards a green and high efficiency direction [8, 9, 10, 11, 12, 13], and the chitosan is a known example in this category.

Chitosan, a natural polymer, is used everywhere due to non-poisonous, multifunctional and excellent biological compatibility [14, 15, 16, 17, 18]. Some chitosan derivatives have the potential to be corrosion inhibitors due to the adsorbable groups in its molecular structure that could bond with metal, such as hydroxyl and amino groups [19, 20]. However, macromolecular chitosan can be dissolved well by diluted acid instead of water so that the inhibition efficiency is very low [21, 22]. Therefore, it is significant to produce a chitosan derivative with the features of good inhibition property, water solubility and pro-environment. Thiourea, as a traditional corrosion inhibitor, has certain inhibition effect. But the inhibition effect of single component thiourea is not good, and there is extreme concentration phenomenon [23, 24, 25]. Most researches have been focused on the modification of chitosan based on introducing thiourea in recent years, which can offer $–NH_2$ and enhance active adsorption points [26, 27]. Notably, researchers pay more attention to the adsorption of thiourea-chitosan for heavy metal ions rather than the inhibition performance, and the solubility of the synthesized thiourea-chitosan is not so well [28, 29].

Thus, the TUCTS with good water solubility and corrosion inhibition property was synthesized based on degraded chitosan (DCS) in this study. FT-IR and elemental analysis were used for characterizing the structure of TUCTS, the corrosion inhibition property and behavior of TUCTS on Q235 steel in 1 $mol \cdot L^{-1}$ HCl were tested by weight loss method, surface morphology analysis and electrochemical measurements.

2. EXPERIMENTAL

2.1 Materials and reagents

DCS was prepared with the raw chitosan as original material. The raw chitosan is a biochemical reagent and from Sinopharm Chemical ReagentCo., Ltd. Thiourea and epichlorohydrin are from Shanghai ling feng chemical reagent co. LTD (Shanghai, China) and Sinopharm Chemical Reagent co. LTD (Shanghai, China), respectively. Reagents used in this study are analytical grade and all solutions are made from reagents and distilled water. The aggressive solution (1 $mol \cdot L^{-1}$ HCl) was prepared by diluting HCl (37%) with distilled water. The descaling liquid consists of 1000 mL hydrochloric acid (1:1) and 20 g hexamethylenetetramine.

Q235 steel is used for the corrosion measurements. The composition (wt. %) of Q235 steel is as follows: C 0.16, Si 0.30, Mn 0.53, P < 0.045, S < 0.055 and Fe balance. The sample of 50 mm × 10 mm × 3 mm is used for weight loss experiment. And the sample of 10 mm × 10 mm × 3 mm which sealed with epoxy resin leaving an area of 1 cm^2 is used for electrochemical measurements. Prior to experiment, the samples of weight loss experiment were successively abraded with 400 and 800 grit silicon carbide papers. While, the samples used for electrochemical measurements were continuously abraded with 400, 800, 1000 and 2000 grit silicon carbide papers. Then rinsed with distilled water, degreased in acetone, dried at room temperature and weighed, finally immersed in the corrosive solution.

2.2 Synthesis of the TUCTS

It must be emphasized that we prepared the TUCTS through two processes. Firstly, we degraded the raw chitosan to get degraded chitosan (DCS) through the method of Yang [30]. The molecular weights of the obtained DCS are around 1200 and its structure is depicted as Fig. 1. Then, the TUCTS was synthesized by these steps below.

The preliminary synthesis method of TUCTS was improved based on Zhou [29]. Firstly, the epichlorohydrin was dissolved in a mixed solution of acetone and distilled water with the volume ratio of 1:1. DCS (2 g) and thiourea were added one after another, stirred the mixed solution for 24 h and 6 h respectively. And then, added further thiourea with stirring for another 4 h. At the end of the reaction, the mixed liquid was evaporated with a vacuum-rotary evaporator to acquire the concentrated liquid. Finally, the solid product was obtained by the precipitation process of the concentrated solution with ethanol. The product was filtrated, washed repeatedly with ethanol and dried in a vacuum oven at 25℃. The synthesis scheme is shown in Fig. 2.

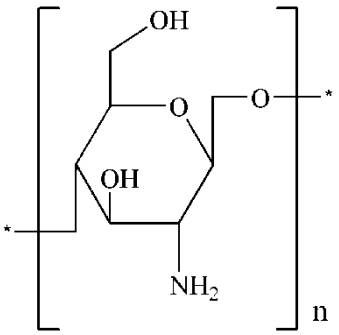

Figure 1. The molecular structure of degraded chitosan (DCS).

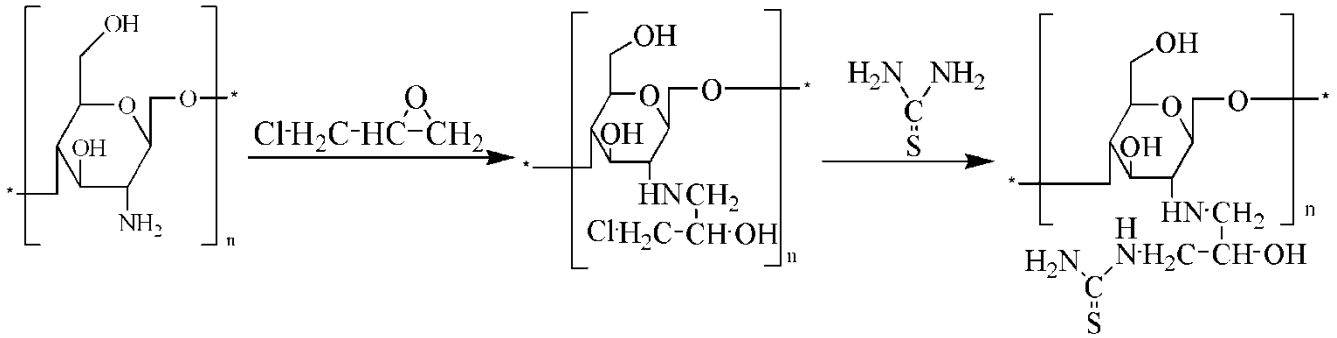

Figure 2. Synthesis route of thiourea-chitosan (TUCTS).

2.3 Characterization of the TUCTS

Fourier transform infrared spectrum (FT-IR) was recorded on a Nicolet 5700 instrument (Nicolet Instrument, Thermo Company, USA). The samples were prepared by grinding with KBr pellet. The spectrums were scanned in the wave number ranged from 4000 cm^{-1} to 400 cm^{-1}.

Elemental analyses were measured on a Vario EL III (Elementar Company, Germany).

2.4 Evaluation of corrosion inhibition performance

The weight loss experiments were performed by immersing Q235 steel in 1 mol·L^{-1} HCl solutions with various concentrations of inhibitor for 6 h at different temperatures. After that, the samples were removed from the test solution, immersed in descaling liquid and ethyl alcohol, finally dried and weighted. All tests were conducted in triplicate and the losses of weight were calculated by taking an average of three values. Preparation and evaluation of the steel specimens were carried out according to ASTM G 1-88 and ASTM G 31-72 [31, 32]. The corrosion rate (ν, g·m^{-2}·h^{-1}) of Q235 steel and the inhibition efficiency (η, %) of inhibitor were calculated by the following equations [33]:

$$\nu = \frac{\Delta W}{St} \quad (1)$$

$$\eta = \frac{\nu_0 - \nu_{inh}}{\nu_0} \times 100\ \% \quad (2)$$

Where ΔW is the average weight loss of Q235 specimens (g); S is the sample area (m^2); t is the immersion time (h); ν_0 and ν_{inh} are the corrosion rates of Q235 steel without and with inhibitors, respectively.

The surface morphology observation was done on a Stereo microscope of Leica DFC490. The surface images of Q235 steel were obtained after 6 h exposure to 1 mol·L^{-1} HCl in the absence and presence of inhibitor.

2.5 Research of corrosion inhibition behavior

Electrochemical measurements were conducted on IM6e Electrochemistry Workstation (ZAHNER, Germany). A three electrode cell was used, with a saturated calomel electrode (SCE) as the reference electrode, a platinum plate as the counter electrode and the Q235 steel as the working electrode. The working electrode was exposed to the test solution with different concentrations of inhibitors at 25℃. Prior to testing, the open circuit potential (OCP) of the working electrode was monitored for 30 min to provide measurements with a steady state condition. All potentials were recorded relative to the SCE.

Polarization curves were carried out by changing the potential from -200 mV to +200 mV vs OCP at a scan rate of 0.5 mV·s^{-1}. The corrosion inhibition efficiency was calculated using the following equation [34]:

$$\eta = \frac{i_0 - i_{inh}}{i_0} \times 100\% \quad (3)$$

Wherein, i_0 and i_{inh} represent the corrosion current densities in the absence and presence of inhibitors, respectively.

Electrochemical impedance spectrum (EIS) was measured with a signal amplitude perturbation of 10 mV at the corrosion potential (E_{corr}) over a frequency ranged from 100 kHz to 50 mHz. The inhibition efficiency (η) was obtained by the equation (4):

$$\eta\% = \frac{R_{ct} - R_0}{R_{ct}} \quad (4)$$

R_{ct} and R_0 are the charge transfer resistance values in the presence and absence of inhibitors, respectively [35].

3. RESULTS AND DISCUSSION

3.1 Characterization of TUCTS

The FT-IR spectra for characterizing the DCS and TUCTS are showed in Fig. 3. It is clearly that the outlines of the two bands are very similar. The broad band at around 3344 cm^{-1} can be seen obviously, which is the inter-molecular and intra-molecular hydrogen bonding of N-H and O-H in the molecules [36]. The original -NH_2 bending vibration absorption peak of DCS at 1599 cm^{-1} disappears in TUCTS [37], but another new absorption peak appears at 1660 cm^{-1}, which indicates that the -NH_2 of DCS reacts with epichlorohydrin and thiourea. Additionally, a new peak at 1275 cm^{-1} in TUCTS derives from the characteristic absorption peak of C=S, which reveals that the thiourea group has been introduced to the -NH_2 of DCS.

The results of elemental analysis are listed in Table 1. N_R%, C_R%, H_R% and S_R% are the actual measured values of mass percentage composition of N, C, H and S. Likewise, N_C%, C_C%, H_C% and S_C% are the theoretical calculated values of mass percentage composition of elements. The actual contents of C, H and N are very close to the theoretical values in DCS, therefore, the constitutional units of homemade degradation chitosan are consistent with the molecular formula of $C_6H_{11}NO_4$. In terms of the distribution of N, the content of N in TUCTS increases to 12.95% from 8.31% in DCS. Meanwhile, the S element is increase newly with a content of 8.69% in TUCTS. These results demonstrate that thiourea radical is introduced to DCS through epichlorohydrin successfully.

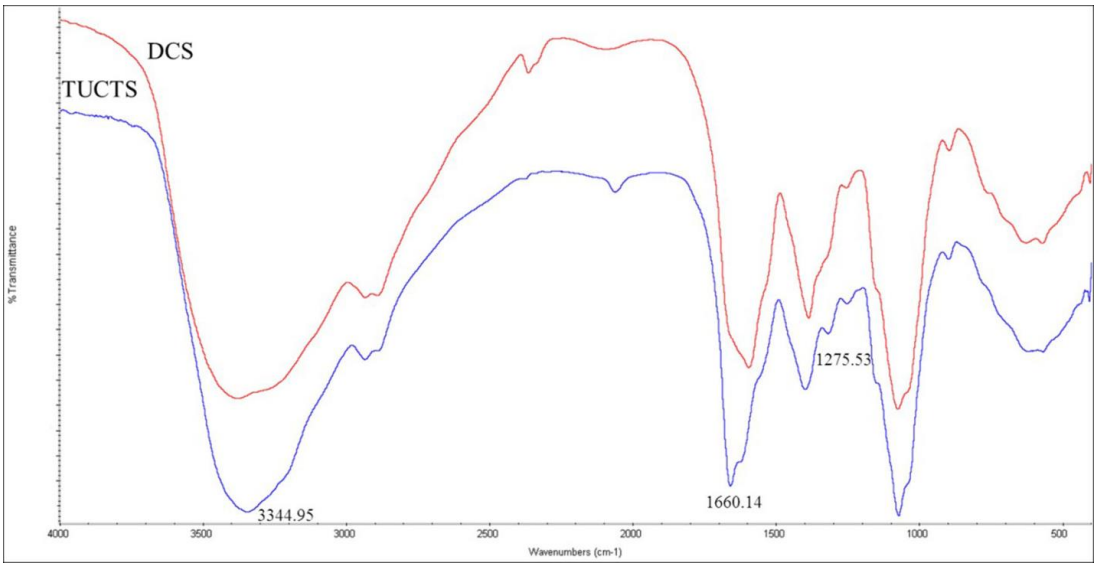

Figure 3. The FT-IR spectra of TUCTS and DCS.

Table 1. The Elemental analysis results of DCS and TUCTS

Sample	Chemical formula	N_R%	N_C%	C_R%	C_C%	H_R%	H_C%	S_R%	S_C%
DCS	$C_6H_{11}NO_4$	8.31	8.69	45.67	44.72	6.61	6.83	-	-
TUCTS	$C_{10}H_{19}N_3O_5S$	12.95	14.33	39.77	40.97	5.83	6.48	8.69	10.92

3.2 Evaluation of corrosion inhibition performance

3.2.1 Weight loss measurements

The corrosion rates of Q235 steel in 1 mol·L^{-1} HCl solutions with various concentrations of TUCTS at different temperatures are showed in Fig. 4. It can be seen obviously that the corrosion rate of Q235 steel increases sharply as the temperature increases in the absence of inhibitor. The increase of temperature accelerates the diffusion of corrosion particles. After adding TUCTS, the corrosion rate decreases significantly. The corrosion rates at 25 ℃ and 40 ℃ are almost the same. However, the corrosion rate is the highest at 80℃. It is likely that the relatively high temperature increases the activation of metal surface so that accelerate the corrosive particles permeating into steel [38].

Fig. 5 illustrates the inhibition efficiency of TUCTS for Q235 steel in 1 mol·L^{-1} HCl solutions with the changes of concentration at different temperatures. From Fig. 5, the presence of a small dosage can inhibit the corrosion of metal at 25℃, which indicates that the water-soluble TUCTS can adsorb on the metal surface quickly. Furthermore, the inhibition efficiency increases with the concentrations of TUCTS increase from 5 mg·L^{-1} to 200 mg·L^{-1} at 25℃, 40℃ and 60℃, proving that the inhibitor is effective again. Nevertheless, a further increase in the inhibitor concentration provides no significant change in the value of the inhibition efficiency due to the adsorption of inhibitor on metal surfaces is approaching saturation [39]. And the efficiency reaches the maximum value (90%) at 400 mg·L^{-1} (25℃ and 40℃). Although the inhibition efficiency of TUCTS declined somewhat at 60℃ in comparison with 25℃ and 40℃, it still can reach 88% at 1000 mg·L^{-1}. Thus, it seems that TUCTS has a good inhibition performance at 60℃. The inhibition efficiency decreases rapidly at 80℃, this is because that molecules move violently at higher temperatures and cause self-desorption.

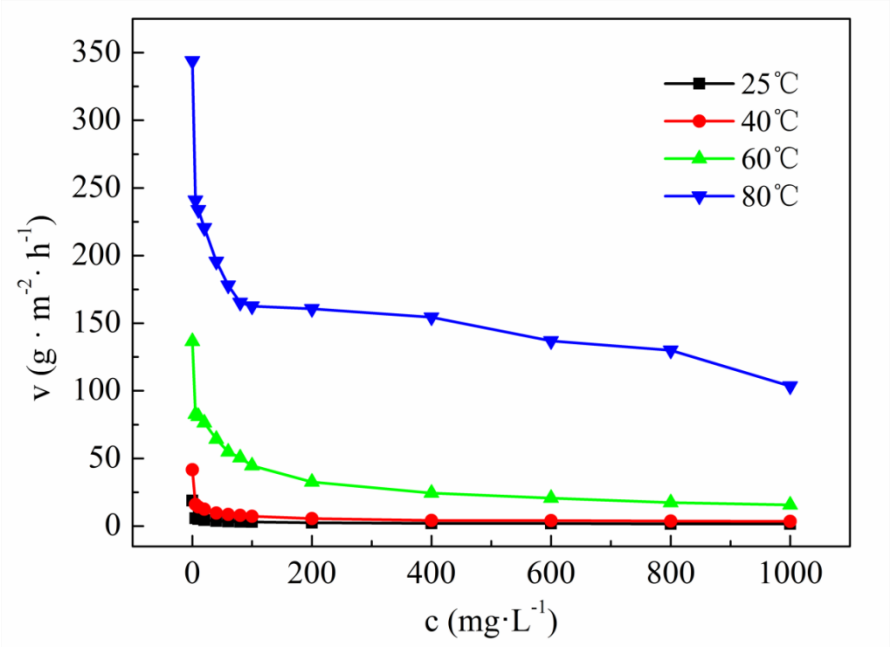

Figure 4. The corrosion rates of Q235 steel in l mol·L^{-1} HCl soltion with various concentrations of TUCTS at different temperatures.

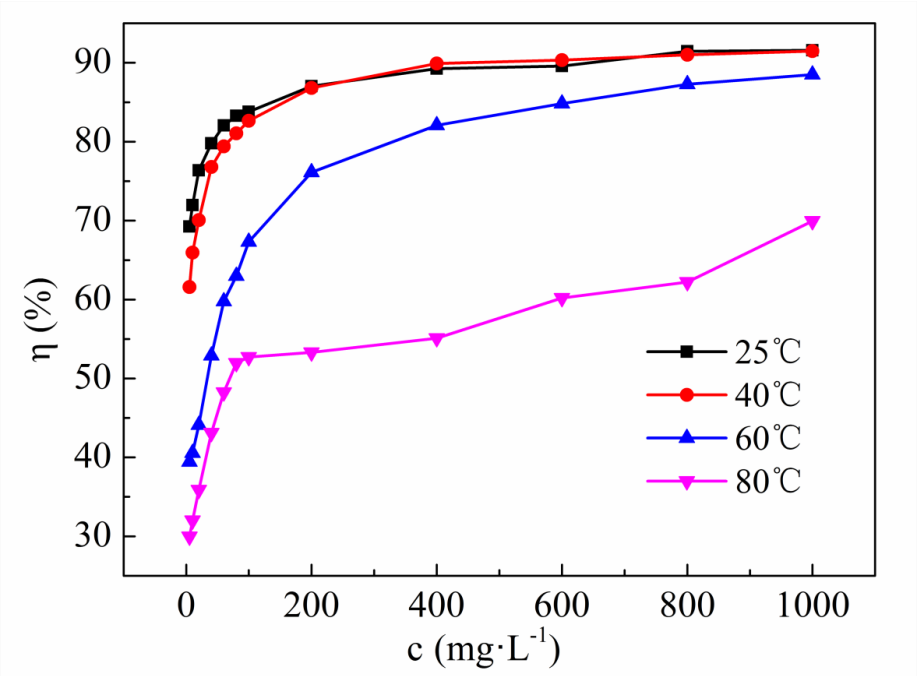

Figure 5. The inhibition efficiency for Q235 steel in l mol·L^{-1} HCl solution with various concentrations of TUCTS at different temperatures.

3.2.2 Surface morphology analysis

The surface morphology of Q235 steel in the absence and presence of 200 mg·L^{-1} inhibitor is magnified as showed in Fig. 6. The Q235 steel is corroded severely without inhibitor so that the pitting corrosion emerges on the lateral face of the Q235 steel at 25℃ and 40℃, respectively.

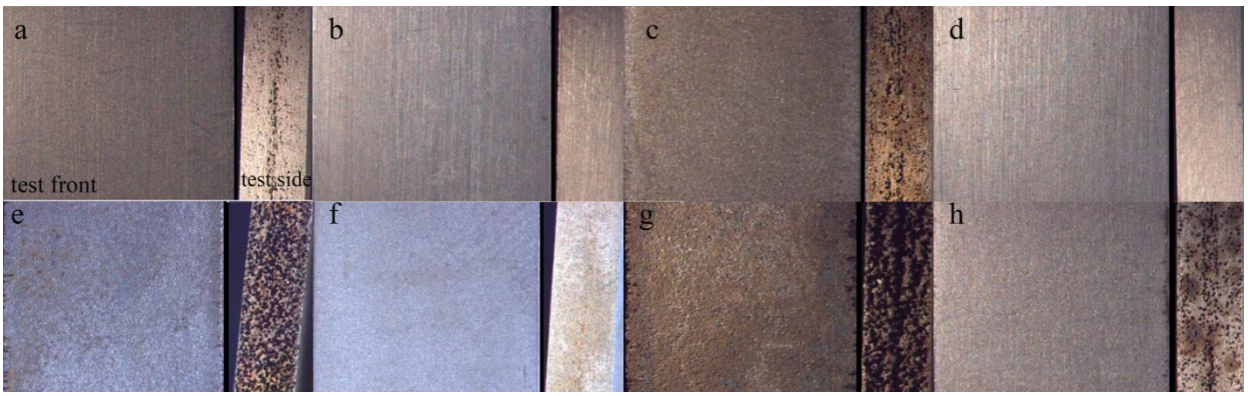

Figure 6. Surface morphology images of Q235 steel (a,c,e,g-in 1 mol/L HCl; b,d,f,h-in 200mg·L^{-1} TUCTS; a,b-25℃; c,d-40℃; e,f-60℃; g,h-80℃).

But, the corrosion phenomenon is dramatically reduced and the pitting corrosion is also restrained after adding TUCTS. From the graph e, the front side of Q235 steel without TUCTS is very rough and the quantity of small holes can be seen on the test side at 60℃. On the contrary, the front side of sample is smooth and no significant pitting corrosion on the side from the graph f, which demonstrates

that TUCTS can inhibit the corrosion of Q235 steel well in hydrochloric acid at 60℃. As seen in graph g, the surface of steel is corroded seriously without the inhibitor at 80℃. Although the front side is very smooth, the corrosion on the test side still exists from the graph h. Besides, the pitting corrosion cannot be inhibited on the lateral face of the Q235 steel, which reveals that the protection efficiency of TUCTS is poor for steel Q235 at 80℃.

3.2.3 Adsorption isotherm

The type of interaction between the inhibitor and the metal surface can be described by the adsorption isotherm. It is known that the adsorption of inhibitor molecules on the metal surface is a substitution process. Thus, the adsorbed water molecules on the metal surface are replaced by inhibitor molecules [40]. In order to gain the mode of adsorption of the inhibitor on the steel surface, various adsorption isotherms were tried. We found that the Langmuir adsorption isotherm is the best fit for describing the adsorption behavior [41]. The Langmuir adsorption isotherm is illustrated as the following equation (5):

$$\frac{C}{\theta} = C + \frac{1}{K_{ads}} \quad (5)$$

Wherein, θ is the surface coverage and from the experimental results of the weight loss; C is the molar concentration of the inhibitor; K_{ads} is the adsorption equilibrium constant and represents the adsorption strength between inhibitors and metal surface, which is related to the standard free energy of adsorption (ΔG^0_{ads}). The equation (6) describes the relationship between K_{ads} and ΔG^0_{ads}:

$$\Delta G^0_{ads} = -RT\ln(55.5K_{ads}) \quad (6)$$

Where 55.5 is the molar concentration of water in the solution [42]; R is the universal gas constant; T is the thermodynamic temperature.

The adsorption isotherms are obtained between C_{inh}/θ versus C_{inh} at various temperatures in Fig. 7. Table 2 provides us with the thermodynamic parameters. It is observed that the linear regression coefficients (R^2) are close to 1 very much, confirming that the adsorption process of TUCTS obeys the Langmuir adsorption model. Thus, the TUCTS molecules can adsorb on the Q235 steel surface and form a film that prevents the metal from the hydrochloric acid corrosion. The negative values of ΔG^0_{ads} are obtained in the presence of inhibitor, suggesting that the adsorption of TUCTS is a spontaneous process and the adsorbed film on the steel surface is stabilized [43]. Meanwhile, the values of ΔG^0_{ads} less than -20 kJ·mol^{-1} signify physisorption, that is electrostatic interaction between the molecules and the metal surface. While the values of ΔG^0_{ads} around -40 kJ·mol^{-1} or more negative represent chemisorptions which arise from the charges sharing or charges transfer between the inhibitor molecules and the metal surface to form a chemistry bond [42]. The calculated values of ΔG^0_{ads} in this test are higher than -40 kJ·mol^{-1} but lower than -20 kJ·mol^{-1} or around -40 kJ·mol^{-1}. So we can speculate that the adsorption process of TUCTS is governed by both chemisorption and physisorption. However, the adsorption process of TUCTS at higher temperature is inclined to chemisorption according to the values of ΔG^0_{ads} at various temperatures. Therefore, the chemical action between TUCTS and metal surface is dominant. The inhibition film is mainly forming through the interaction between the metal atoms and some atoms in TUCTS molecule. The values of enthalpy and entropy of adsorption process can be calculated by the

Van't Hoff equation (7) and the equation (8), respectively. The equation (8) is written by the definition of the Gibbs free energy:

$$\ln K_{ads} = -\frac{\Delta H^0_{ads}}{RT} + \text{constant} \quad (7)$$

$$\Delta G^0_{ads} = \Delta H^0_{ads} - T\Delta S^0_{ads} \quad (8)$$

The adsorption process of TUCTS on Q235 steel surface is exothermic and spontaneous from the negative value of enthalpy and the positive value of entropy [44]. On this basis, we conclude that lower temperature is more favorable for adsorption and the inhibitor exhibits better corrosion inhibition performance. The results are consistent with the weight loss and stereomicroscope analysis.

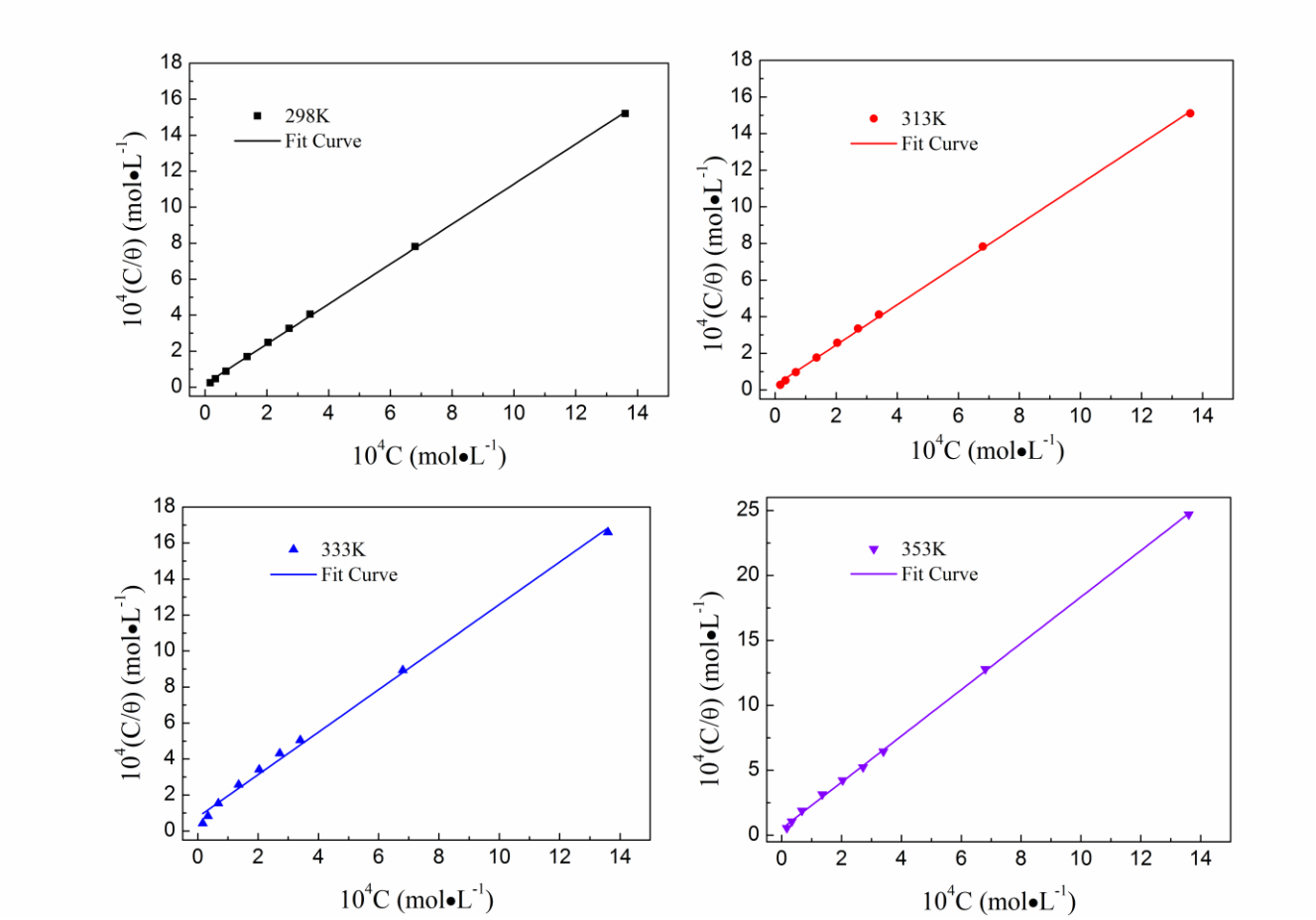

Figure 7. Langmuir adsorption plots for Q235 steel in 1 mol·L^{-1} HCl containing various concentrations of TUCTS at different temperatures.

Table 2. Thermodynamic analysis of different temperatures for Q235 steel in 1 mol·L^{-1} HCl containing various concentrations of TUCTS.

T/K	Slope	R^2	K_{ads}	ΔG^0_{ads} (kJ·mol^{-1})	ΔH^0_{ads} (kJ·mol^{-1})	ΔS^0_{ads} (kJ·mol^{-1})
298	1.1136	0.9997	5.88×10^4	-37		
313	1.1012	0.9994	3.96×10^4	-38	-21*	
333	1.1787	0.9958	1.28×10^4	-37	-20#	0.056#
353	1.7805	0.9995	1.93×10^4	-41		

*Parameters calculated from equation (7); #Parameters calculated from equation (8)

3.3 Behavior of corrosion inhibition

3.3.1 Potentiodynamic polarization analysis

Fig. 8 illustrates the potentiodynamic polarization curves of Q235 steel specimens in 1 mol·L^{-1} HCl solution containing various concentrations of TUCTS at 25℃. The relevant electrochemical parameters including corrosion potential (E_{corr}), cathode and anode Tafel slopes (b_c, b_a) and corrosion current density (i_{corr}) are obtained by the Tafel extrapolation method. The electrochemical parameters and calculated inhibition efficiency (η) are summarized in Table 3.

The corrosion current density is decreased from 537 μA·cm^{-2} in uninhibited solution to 111 μA·cm^{-2} with the addition of 10 mg·L^{-1} TUCTS and gets reduced gradually with the concentration of the inhibitor increases, indicating that the presence of TUCTS impedes the corrosion of the Q235 steel effectively. The cathode polarization current density decreases with the concentration at the same potential. However, the anode polarization current density has a slight increase at more positive potentials when the concentration exceeds 100 mg·L^{-1}. It seems that the inhibitor is more inclined to inhibit the corrosion reaction of cathode.

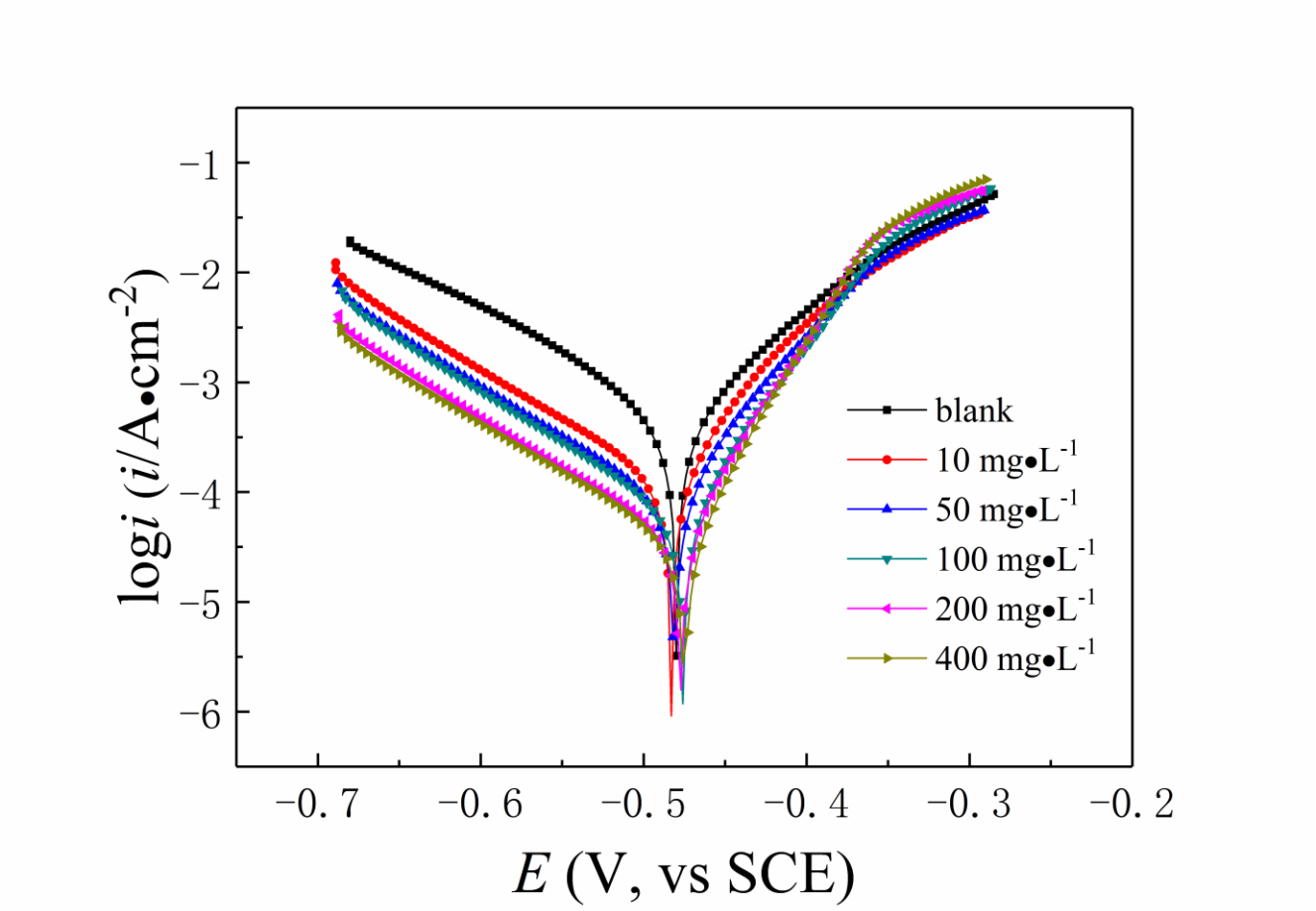

Figure 8. Potentiodynamic Polarization curves for Q235 steel in 1 mol·L^{-1} HCl in the absence and presence of different concentrations of inhibitor at 25℃.

Table 3. Potentiodynamic Polarization parameters for Q235 steel in 1 mol·L^{-1} HCl in the absence and presence of different concentrations of inhibitor at 25℃

c (mg·L^{-1})	b_a (mV·dec^{-1})	$-b_c$ (mV·dec^{-1})	I_{corr} (μA·cm^{-2})	E_{corr} (vs SCE) (mV)	η (%)
blank	79	124	537	-480	-
10	73	110	111	-483	79
50	65	109	76	-482	86
100	59	108	58	-476	89
200	56	109	36	-477	93
400	52	114	34	-476	94

From the Table 3, the inhibition efficiency increases with the concentration of TUCTS and reaches a maximum value of 94% at 400 mg·L^{-1}. Considering the slight shift of anode and cathode Tafel slopes in the presence of inhibitors compare with the blank solution, the anode and cathode reactions are affected almost equally and the reaction inhibition mechanism is unaltered. The deviation values of corrosion potential of X65 steel in inhibited solution are tiny relative to the blank solution. Hence, TUCTS acts as a mixed-type inhibitor with an inhibition effect by geometrical blanketing effect, which is consistent with the concept of geometrical blanketing effect as C.N. Unnisa depicted [45, 46]. For the corrosion inhibitor which inhibition mechanism belongs to geometrical blanketing effect, it could block the anodic and cathodic sites where the corrosion reaction takes place without transforming the corrosion mechanism [47]. Above all, it is concluded that TUCTS is a mixed-type inhibitor. The inhibitor can reduce the anode dissolution of Q235 steel, but it is more beneficial to inhibit cathode hydrogen evolution reaction simultaneously.

3.3.2 Electrochemical impedance spectrum analysis

Electrochemical impedance spectra are analyzed to research the inhibition mechanism of TUCTS. Impedance spectra for X65 steel in 1 mol·L^{-1} HCl without and with various concentrations of TUCTS at 25℃ are showed in Fig. 9 and Fig. 10. The Nyquist plots are all semicircle capacitive loops, the shapes of impedance plots for X65 steel with the concentration of inhibitor are nearly identical. In addition, it can be found that there is one time constant over the whole frequency range in Bode plots obviously. Accordingly, the obtained Nyquist plots exhibit a degradation phenomenon and present a single capacitive loop [48], implying that the mechanism of corrosion reaction is invariable even if in the addition of TUCTS. As shown in Figure 9, the addition of inhibitor results in the increase of diameter of capacitive loop significantly and the diameter enlarges further with the concentration. This proves that the corrosion reaction is obstructed owing to the formation of an adsorbed layer. The impedance modulus (Z) at low frequency in Bode plots increase clearly with the increase of inhibitor concentration, which suggests that the diffusion process of cathode hydrogen evolution is inhibited due to the coverage of adsorption film. In the intermediate and high frequency region, the impedance modulus shows a linear

relationship with the frequency and the slope increases with the concentration of inhibitor. Meanwhile, the maximum phase angle (around 80°) is increased by increasing the concentration of inhibitor because of the density of surface or the incrassate adsorption membrane [49]. Thus, the corrosion process can be under control.

The equivalent electric circuit in Fig. 11 is used to fit the relevant parameters of the electrochemical system. Hereinto, R_s is the solution resistance; R_{ct} represents the charge transfer resistance; CPE is the constant phase element and considered to be made up of double layer capacitance (C_{dl}) and dispersion exponent (n). The impedance fitting results and the calculated inhibition efficiency are listed in Table 4. From the Table 4, R_{ct} is proportional to the concentration of inhibitor but C_{dl} is opposite. The increase of R_{ct} reveals that the adsorbed inhibitor molecules inhibit the charge transfer reaction strongly. The water molecules are substituted by the adsorbed inhibitor molecules, which might result in a decrease in local dielectric constant, and thus C_{dl} is decrease [40]. The values of *n* in the presence of inhibitor are around 0.90 compared to the blank 0. 8. The change of *n* shows that the steel surface becomes more uniform in the presence of inhibitor [50]. In general, TUCTS exhibits inhibition performance well by adsorbing on the Q235 steel surface and taking shape the protective films further. The EIS measurements are agree with the results of potentiodynamic polarization curves and weight loss.

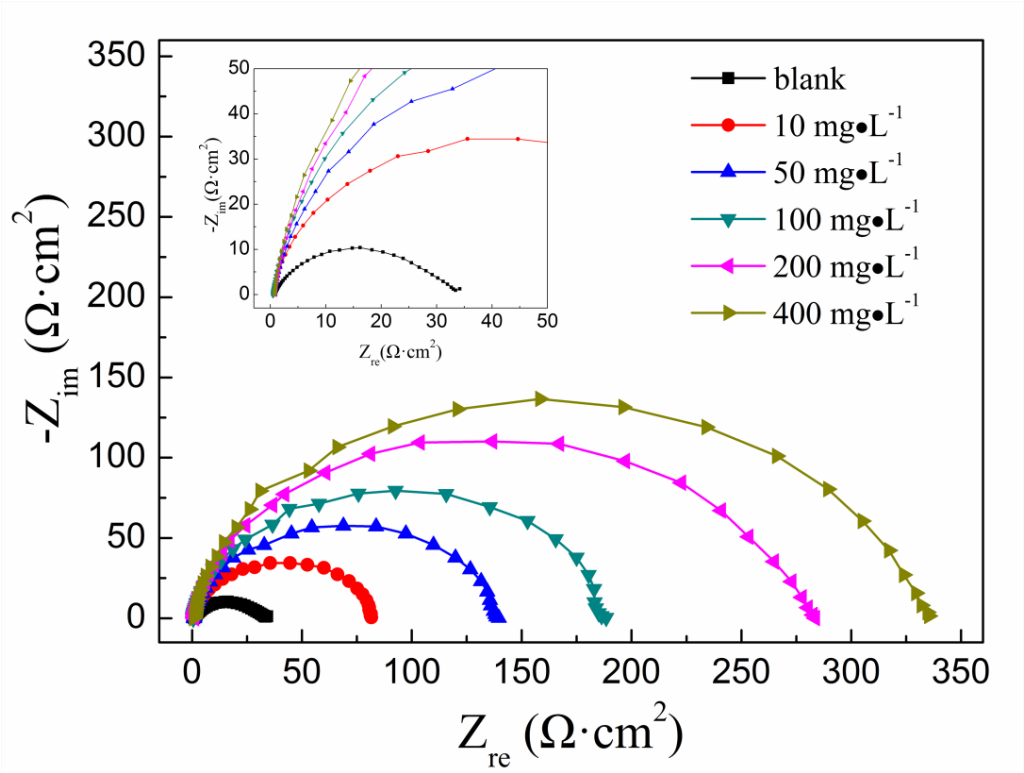

Figure 9. Nyquist plots for Q235 steel in 1 mol·L^{-1}HCl with different additions of the TUCTS at 25℃.

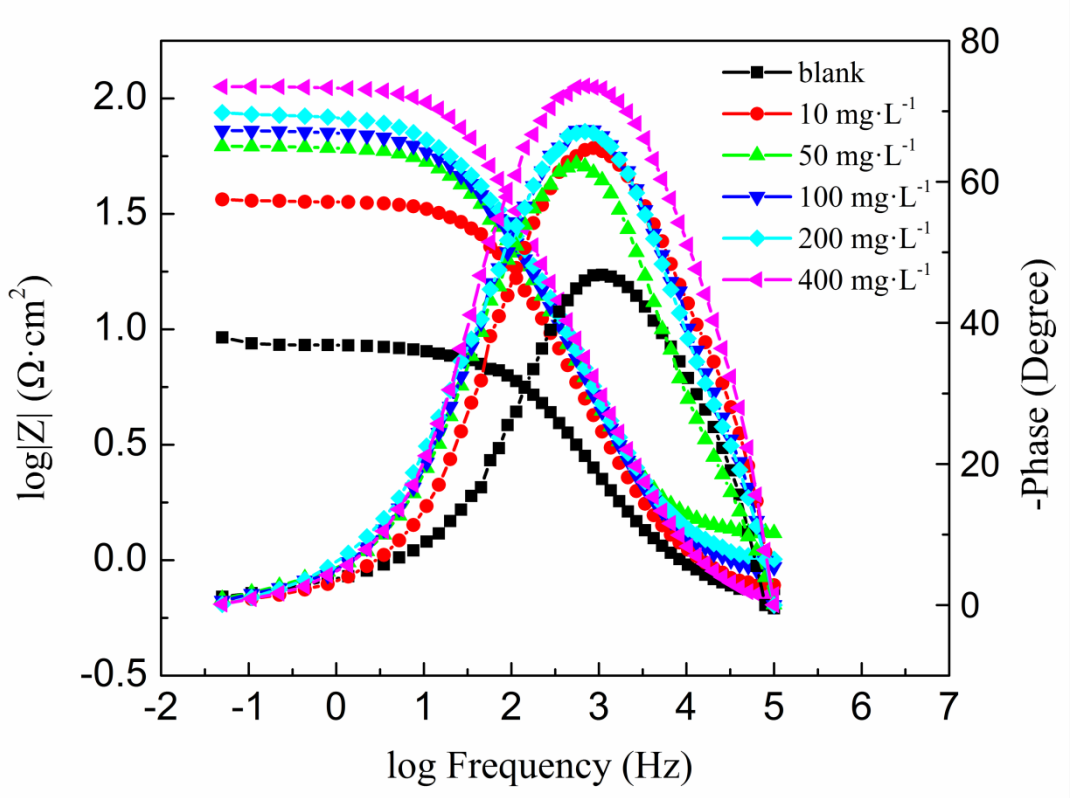

Figure 10. Bode plots for Q235 steel in 1 mol·L^{-1} HCl with different additions of the TUCTS at 25℃.

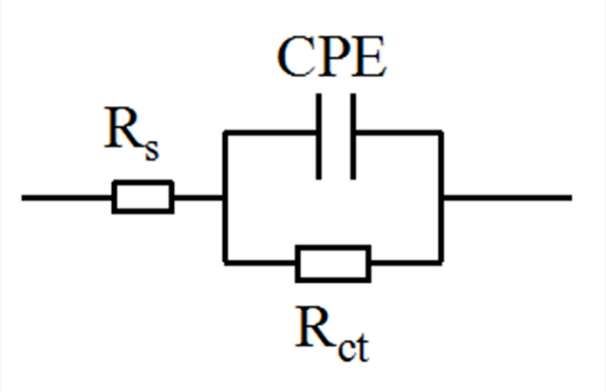

Figure 11. The equivalent circuit model for fitting the EIS data.

Table 4. Electrochemical parameters for Q235 steel in 1 mol·L^{-1} HCl with different additions of the TUCTS at 25℃.

c (mg·L^{-1})	R_s (Ω·cm^{-2})	R_{ct} (Ω·cm^{-2})	C_{dl} (μF·cm^2)	n	η (%)
blank	0.81	32	341	0.8	-
10	0.57	83	108	0.9	62
50	0.79	140	88	0.9	77
100	0.50	183	65	0.9	83
200	0.86	272	62	0.9	88
400	0.64	328	57	0.9	90

3.3.3 Effect of immersion time

The EIS spectra of Q235 steel in 1 mol·L^{-1} HCl containing 200 mg·L^{-1} TUCTS at different immersion time at 25℃ are obtained for evaluating the persistence of inhibition effect and the change law of adsorption film over time, as showed in Fig. 12 and Fig. 13. From Nyquist diagram, the depressed capacitive semicircle arc could be seen in addition of inhibitor. It is noted that the diameter of capacitive loop increases distinctly in the presence of inhibitor after 0.5 h, indicating the TUCTS possess a quick inhibition effect. The diameter is an initial increase by increasing the immersion time prior to 24 h and then a decrease with time elapsing, which is caused by the process of absorption and desorption of inhibitor. To make it clearly that illustrating the interaction between corrosion inhibitor and metal with time, the relevant parameters of fitting for the impedance spectra refer to the equivalent circuit (Fig 11) are summarized and listed in Table 5. Based on the fitting parameters, R_{ct} is increase significantly but C_{dl} is opposite in the presence of inhibitor ahead of 24 h, suggesting that the inhibitor molecules take place of water molecules constantly, form the protective film and enlarge the coverage, which could result in the hamper for corrosion reaction. On the other hand, the R_{ct} decrease a bit and the C_{dl} enlarge slightly from 48 h to 168 h, which reveals that the resistance of corrosion reaction decrease owing to the attenuation of adsorption film [51]. Furthermore, it is observed clearly that the values of *n* are almost invariant in addition of the inhibitor, indicating the compactness of working electrode surface in comparison with to the absence of the inhibitor. Based on what we have discussed previously, the TUCTS can provide protection up to 168 h.

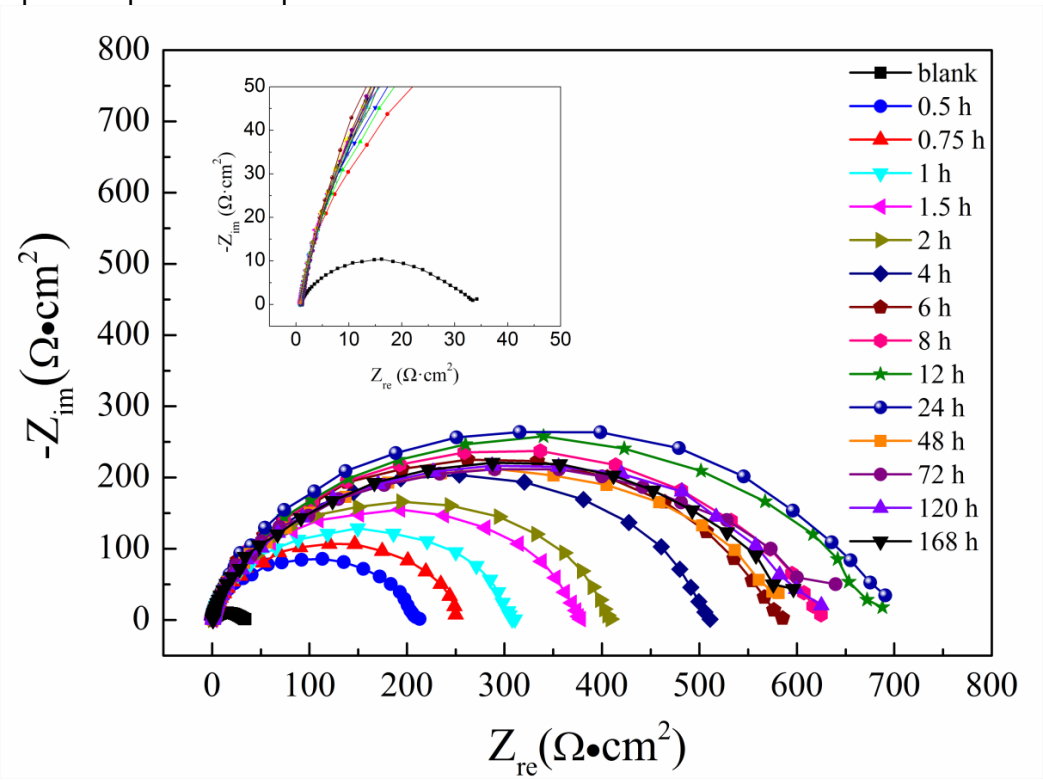

Figure 12. Nyquist plots of various immerse time for Q235 steel in 1 mol·L^{-1} HCl with 200 mg·L^{-1} TUCTS at 25℃.

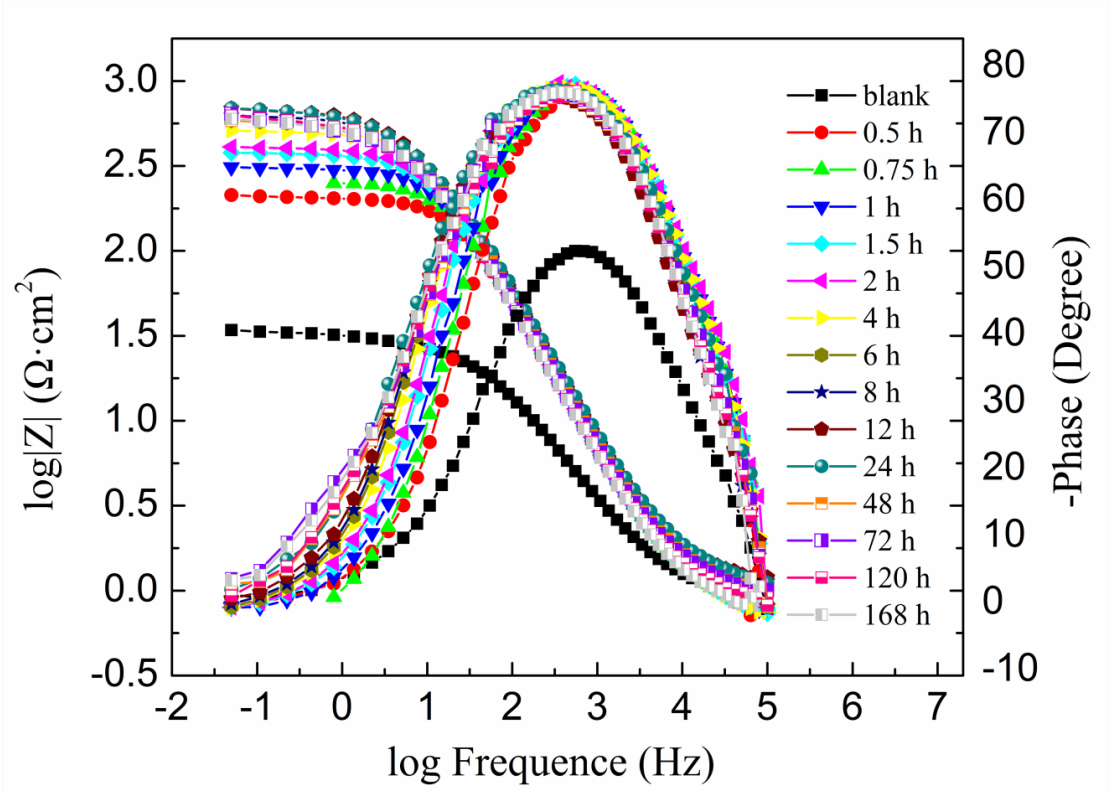

Figure 13. Bode plots of various immerse time for Q235 steel in 1 mol·L^{-1} HCl with 200 mg·L^{-1} TUCTS at 25℃.

Table 5. Electrochemical parameters of different immerse time for Q235 steel in 1 mol·L^{-1} HCl with 200 mg·L^{-1} TUCTS at 25℃.

t (h)	R_s (Ω·cm^2)	R_{ct} (Ω·cm^2)	C_{dl} (μF·cm^{-2})	n	η(%)
blank	0.81	32	341	0.8	-
0.5	0.70	209	81	0.9	85
0.75	0.70	260	76	0.9	88
1	0.71	309	64	0.9	90
1.5	0.70	377	62	0.9	92
2	0.70	410	61	0.9	92
4	0.69	507	61	0.9	94
6	0.87	571	61	0.9	94
8	1.01	609	60	0.9	95
12	1.07	663	64	0.9	95
24	0.98	677	64	0.8	95
48	0.90	559	74	0.9	94
72	0.87	579	77	0.9	95
120	0.83	584	77	0.9	95
168	0.85	564	81	0.9	94

4. CONCLUSIONS

The paper puts forward the synthesis process of corrosion inhibitor thiourea-chitosan (TUCTS) based on degraded chitosan (DCS). The FT-IR and elemental analysis results confirm that the thiourea group could be introduced into the DCS through epichlorohydrin successfully. TUCTS exhibits fine corrosion inhibition effect for Q235 steel by forming adsorption film. The adsorption process of the TUCTS obeys the Langmuir adsorption isotherm. It's a spontaneous and mixed adsorption dominated by chemisorption. Electrochemical measurement results reveal that the TUCTS is a mixed-type inhibitor, that both the cathode and anode corrosion reactions are hampered. The adsorbed inhibition molecules replace the corrosive molecules ceaselessly on metal surface and form extensive coverage area. Electrochemical impedance spectra analysis result suggests that the TUCTS can provide protection up to 168 h.

ACKNOWLEDGMENTS
The authors gratefully acknowledge the financial support of the Natural Science Foundation of Shandong Province of China (Project No. ZR2013EMQ015) and the Fundamental Research Funds for the Central Universities (Project No. 201713060).

References

1. I.B. Obot, N.K. Ankah, A.A. Sorour, Z.M. Gasem and K. Haruna, *SM&T*., 14(2017) 1.
2. J. Aljourani, M.A. Golozar and K. Raeissi, *Mater Chem Phys*., 121(2010) 320.
3. M.A. Bedair, M.B. El-SabbahM, A.S. Fouda and H.M. Elaryian, *Corros Sci*., 128(2017) 54.
4. Z. Yang, F.T. Zhan, Y.Pan, Z.F. LYu and C.Y. Han, *Corros Sci*., 99(2015) 281.
5. P. Morales-Gil, M.S. Walczak, R.A. Cottis, J.M. Romero and R. Lindsay, *Corros Sci*., 85(2014) 109.
6. H.H. Zhang and Y. Chen, *J Mol Struct*., 1177(2019) 90.
7. Y.E. Bakri, L. Guo, E.H. Anouar and E.M. Essassi, *J Mol Liq*., 274(2019) 759.
8. G.M. Al-Senani, *Int J Electrochem Sci.*, 11 (2016) 291.
9. K. Azzaoui, E. Mejdoubi, S. Jodeh, A. Lamhamdi and E. Rodriguez-Castellón, *Corros Sci*., 129(2017) 70.
10. L. Vrsalović, S. Gudić, D. Gracić, I. Smoljko, I. Ivanić, M. Kliškić and E.E. Oguzie, *Int J Electrochem Sci.*, 13 (2018) 2102.
11. M. Mobin, M. Basik and J. Aslam, *J. Measurement,* 134(2019) 595.
12. M. Mobin, M. Basik and M.A. Shoeb, *Appl Surf Sci*., 469(2019) 387.
13. M. Chevalier, M. Lebrini, F. Robert, S. Sutour, F. Tomi, C. Jama, F. Bentiss and C. Roos, *Int J Electrochem Sci.*, 14 (2019) 1208.
14. H.E. Knidri, R. Belaabed, A. Addaou, A. Laajeb and A. Lahsini, *Int J Biol Macromol*., 120(2018) 1181.
15. M. A. M. Rocha, M. A. Coimbra and C. *Nunes, Curr Opin Food Sci.*, 15(2017) 61.
16. Z.E. Bistgani, S.A. Siadat, A. Bakhshandeh, A.G. Pirbalouti and M. Hashemi, *The Crop J.*, 5(2017) 407.
17. M. Larsson, W.C. Huang, M.H. Hsiao, Y.J. Wang, M. Nydén, S.H. Chiou and D.M. Liu, *Prog Polym Sci.*, 38(2013) 1307.
18. J.A. Mukta, M. Rahman, A.A. Sabir, D.R. Gupta, M.Z. Surovy, M. Rahman and M. T. Islam, *Biocatalysis and Agricultural Biotechnol.*, 11(2017) 9.

19. S. Nofrizal, A.A. Rahim, B. Saad, R.P. Bothi and A.M. Shah, *Metall Mater Trans A*., 43(2012)1382.
20. J.L. Wang and C. Chen, *Bioresour Technol.*, 160(2014) 129.
21. M.H.M. Hussein, M.F. El-Hady, H.A.H. Shehata, M.A. Hegazy and H.H.H. Hefni, *J Surfactants Deterg*., 16(2013) 233.
22. A.M. Fekry and R.R. Mohamed, *Electrochim Acta*, 55(2010) 1933.
23. F. Kuang, T.H. Shi, J. Wang and F. Jia, *J Solid State Electr.*, 13(2009) 1729.
24. V.V. Torres, V.A. Rayol, M. Magalhães, G.M. Viana and L.C.S. Aguiar, *Corros Sci*., 79(2014) 108.
25. B.G. Ateya, B.E. El-Anadouli and F.M. El-Nizamy, *Corros Sci*., 24(1984) 497.
26. A. Ramesh, H. Hasegawa, W. Sugimoto, T. Maki and K. Ueda, *Bioresource Technol*., 99(2008) 3801.
27. A.P. Zhu, M.B. Chan-Park, S. Dai and L. Li, *Colloids Surf B: Biointer*., 43(2005) 143.
28. L.L. Fan, C.N. Luo, Z. Lv, F.G. Lu and H.M. Qiu, *J Hazard Mater*., 194(2011)193.
29. L.M. Zhou, J.H. Liu and Z.R. Liu, *J Hazard Mater*., 172(2009) 439.
30. X.G. Yang, L.Y. Shao, S.F. Zhang, W. Jiao and Y.T. Li, *J of Chinese Society for Corrosion and Protection*., 28(2008) 325.
31. ASTM G 01-03, ASTM Book of Standards, vol. 3.02. West Conshohocken, PA. (2003).
32. ASTM G 31-72, ASTM Book of Standards, vol. 3.02. West Conshohocken, PA. (2004).
33. A. Salhi, S. Tighadouini, M. El-Massaoudi, M. Elbelghiti, A. Bouyanzer, S. Radi, S.E. Barkany, F. Bentiss and A. Zarrouk, *J Mol Liq.*, 248(2017) 340.
34. V. Hemapriya, M. Prabakaran, K. Parameswari, S. Chitra, S.H. Kim and I.M. Chung, *J Ind Eng Chem.*, 40(2016) 106.
35. S.T. Zhang, Z.H. Tao, S.G. Liao and F.J. Wu, *Corros Sci.*, 52(2010) 3126.
36. A.A. Tayel, S.I.A. Ibrahim, M.A. Al-Saman and S.H. Moussa, *Int J Biol Macromol.*, 69(2014) 471.
37. X.Q. Feng, X.F. Li, S. Yang and J.F. Zhang, *Natural Product Research and Dev*., 24(2012)1075.
38. Y.J. Liu, Z.M. Gao, X.B. Lu and L.Q. Wang, *Int J Electrochem Sci.*,14 (2019) 150.
39. O. Olivares-Xometl, N.V. Likhanova, M.A. Dominggues-Aguilar and E. Arce, H. Dorantes, *Mater Chem Phys*., 110(2008)34.
40. J. Zhang, F.M. Zhu, W.W. Song and M. Du, *J Surfactants Deterg*., 16(2013) 559.
41. A. Espinoza-Vazquez and F. J. Rodr´ıguez-Gomez, *RSC Adv*., 6(2016)70226.
42. A. Singh, K.R. Ansari, X. Xu, Z. Sun and A. Kumar, *Sci Rep-UK*., 7(2017) 10904.
43. E.E. Ebenso and I.B. Obot, *Int J Electrochem Sci*., 5(2010) 2012.
44. I. Ilim, S. Bahri, W. Simanjuntak, Y.M. Syah and B. Bundjali, *J. Mater. Environ. Sci.,* 8(2017) 2381.
45. C.N. Unnisa and S. Chitr, *J Environ Chem Eng*., 6(2018) 6714.
46. A. Yurt, B. Duran and H. Dal, *Arab J Chem*., 7(2014) 732.
47. E. Ituen, O. Akaranta and A. James, *J Mol Liq.*, 224 (2016) 408.
48. J. Wang, C.N. Cao and J.J. Chen, *Corrosion Science and Protection Technol*., 4(1992) 79.
49. J. Porcayo-Calderon, E.M. Rivera-Muñoz, C. Peza-Ledesma, M. Casales-Diaz and L.M. Martínez dela Escalera, *J. Electrochem. Sci. Technol.,* 8(2017)133.
50. H. Tian, W. Li, B. Hou and D. Wang, *Corros Sci*., 117(2017) 43.
51. J. Zhang, M, Du, H.H Yu and N. Wang, *Acta Phys-Chim Sin.*, 25(2009) 525.